Chinese Chemical Letters 33 (2022) 1681–1692

Contents lists available at ScienceDirect

Chinese Chemical Letters

journal homepage: www.elsevier.com/locate/cclet

Diketopyrrolopyrrole-derived organic small molecular dyes for tumor phototheranostics

Qianli Ma[a], Xu Sun[a], Weili Wang[a], Dongliang Yang[a], Cangjie Yang[b], Qian Shen[a], Jinjun Shao[a,*]

[a] Key Laboratory of Flexible Electronics (KLOFE) & Institute of Advanced Materials (IAM), Nanjing Tech University (NanjingTech), Nanjing 211800, China
[b] Department of Chemistry, Boston College, Chestnut Hill, Massachusetts 02467, United States

ARTICLE INFO

Article history:
Received 23 July 2021
Revised 14 October 2021
Accepted 19 October 2021
Available online 26 October 2021

Keywords:
Diketopyrrolopyrrole
Phototherapy
Photodynamic
Photothermal
NIR dye

ABSTRACT

Cancer is one of the leading causes of human death around the world. Phototherapy, including photodynamic therapy (PDT) and photothermal therapy (PTT), is an emerging light-triggered cancer treatment and shows the advantages of non-invasiveness and low side effects. The design and preparation of efficient phototherapeutic agents are of great significance for phototherapy. Diketopyrrolopyrrole (DPP) is a small molecular organic dye featuring outstanding photophysical properties, facile tuning of structures and properties, and excellent photostability; thus, phototherapeutic agents based on organic small molecular DPP derivatives have attracted significant research attention for not only phototherapy but also photodiagnosis of fluorescence imaging (FLI) and photoacoustic imaging (PAI). This review summarizes the recent progress of various DPP-based organic small molecules on phototheranostics during the last five years. The molecular structure design and their phototheranostics performances are discussed in detail, as will be of great help for further creation of DPP-based phototheranostics.

1. Introduction

According to the World Health Organization (WHO) data, cancer is one of the leading causes of death globally, with an estimated amount of 9.6 million in 2020 [1]. Currently, a tremendous amount of research has been done to develop and/or optimize the current cancer treatment approaches, such as radiation therapy, chemotherapy, and surgery, to improve the anti-tumor efficacy and minimize the adverse effect [2]. For instance, traditional therapeutic strategies often result in an increased cancer cell tolerance threshold, psychological trauma, ineffective treatment, damage to healthy tissues, *etc.*, which brings great pains to the patients [3]. Therefore, tumor phototheranostics with the features of non-invasiveness and high selectivity have gained significant attention for the development of biomedicine [4–9].

Phototheranostic platform is generally a synergetic combination of optical imaging and phototherapy. Usually, phototherapy is mainly consisting of photothermal therapy (PTT) and photodynamic therapy (PDT). PDT has aroused tremendous interest in tumor ablation and anti-bacteria in recent years due to its non-invasiveness, low systemic toxicity, and high tumor selectivity [10]. Generally, the PDT process takes advantage of cytotoxic reactive oxygen species (ROS) to kill cancer cells, when the photosensitizers are irradiated with a proper excitation light source to produce the triplet state (T_1) from singlet state (S_1) *via* intersystem crossing (ISC) (Fig. 1) [11,12]. Currently, most PDT goes through an energy transfer pathway to generate singlet oxygen for the induction of tumor cell apoptosis and/or necrosis, and this pathway is termed type II PDT [13]. And the generation of singlet oxygen is highly dependent on the tissue oxygen concentration. Nonetheless, the hypoxic tumor microenvironment and O_2-consumption during PDT will severely weaken the therapeutic efficacy of type II PDT [14]. Distinct from the type II PDT with severe oxygen dependence, type I PDT is an electron transfer process with less oxygen-dependence, owing to the fact that disproportionation or Haber-Weiss/Fenton reaction will take place to mainly generate superoxide radical ($O_2^{\bullet-}$) and hydroxyl radical ($OH^{\bullet}$) to improve the anti-tumor efficacy [15–18].

As a minimally invasive strategy, PTT has also attracted much attention in recent years [19,20]. The heat generated *via* the non-radiative decay of the therapeutic agent under near-infrared (NIR) light irradiation can selectively kill cancer cells with less damage to the surrounding healthy tissues. An effective photothermal agent should have intensive NIR absorption, high photothermal

* Corresponding author.
E-mail address: iamjjshao@njtech.edu.cn (J. Shao).

https://doi.org/10.1016/j.cclet.2021.10.054
1001-8417/

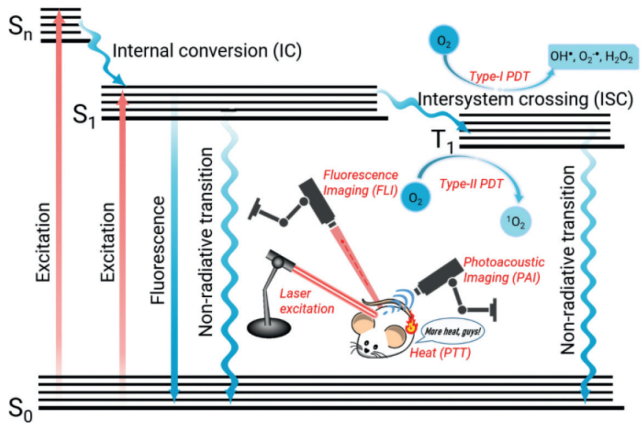

Fig. 1. Illustration of the Jablonski energy diagram for phototherapeutic agents.

conversion efficiency, outstanding photostability, and excellent biosafety [21,22]. To optimize treatment effectiveness, imaging-guided cancer therapy has been extensively adopted, since the spatial distribution and physical size of the tumors are available in real-time. Simultaneously, the accumulation and retention of the phototherapeutic nanoagent at the tumor site can be tracked and quantified for precise inspection and treatment.

Fluorescence imaging (FLI) is an emerging imaging technique that has attracted widespread research attention for its high sensitivity, excellent specificity, and easy operation [23,24]. FLI is based on the fluorescence emission signals coming from the fluorescent phototheranostic agent. The ground state (S_0) photosensitizer absorbs specific light energy upon photoirradiation and jumps to the excited state (S_n). Then, through internal conversion and vibrational relaxation, the excited state decays to the lowest singlet state (S_1), which subsequently returns to the ground state and releases energy in the form of photon radiation; the light emitted is termed fluorescence (Scheme 1) [25–27]. An ideal fluorophore used for FLI usually takes the below factors into consideration, including fluorescence emission wavelength, fluorescence quantum yield (ϕ_{FI}), brightness, photostability, and biosafety.

Photoacoustic imaging (PAI) is based on the ultrasound waves generated by thermoelastic tissue expansion, which is coming from the photothermal effect of the phototheranostic agent under photoirradiation [28–30]. Particularly, PAI and PTT show inherent dependence on the photothermal activity of the phototherapeutic agents; thus, lots of research interest has been devoted to developing the NIR theranostic agents with high photothermal conversion efficiency for PAI-guided PTT towards anti-cancer and antibacterial treatment. The resolution of PAI depends on the arrival time of the ultrasound signals so that three-dimensional images can be obtained without mechanical scanning in the vertical direction. PAI has the potential for multi-scale imaging of biological systems, which presents far-reaching significance for cancer diagnosis.

The phototheranostic agent is critical for optical imaging and phototherapy, which has received considerable research attention. At present, many inorganic nanomaterials with anti-tumor properties have been developed, such as inorganic noble metal nanomaterials (such as Au, Pt), carbon-based nanomaterials, transition metal oxides/sulfides; However, the nature of poor biodegradability and potential long-term biotoxicity of the inorganic phototheranostic agents significantly restrain their future clinical transformation [31–35].

On the contrary, organic molecules with favorable biosafety have been widely used as phototheranostic agents in optical imaging and phototherapy. The organic semiconducting polymeric molecules show the uncertainty in molecular structures and hamper their further clinical application [36,37]. Instead, π-conjugated small molecular organic dyes, with well-defined chemical structures, easy structure tunability, controllable synthetic routes, and excellent biocompatibility, come into the researchers' view and have received increasing attention [19,38,39]. For example, two small molecular organic dyes of indocyanine green (ICG) (λ_{em} = 822 nm, in H_2O) and methylene blue (MB) (λ_{em} = 686 nm, in H_2O) have been approved by the US Food and Drug Administration (FDA) for clinical use [40]. As a matter of fact, all the existing photosensitizers approved for clinical use are organic small molecules till now. However, they suffer the drawback of easy photobleaching. In recent years, many small molecular photosensitizers, such as DPP (diketopyrrolopyrrole), BODIPY (borondipyrromethene), squaraine, and cyanine, have been widely explored [41,42]. And DPP-derivatives shine in the field of tumor diagnosis and treatment thanks to its easy structure tunability, excellent photostability, and photothermal stability [43].

DPP is a lactam-structured π-conjugated organic molecule with high planarity and electron-deficiency, which can conjugate with various electron donors, such as phenyl, thienyl, or furanyl units, to construct the donor-acceptor-donor (D-A-D) structured NIR dyes. Furthermore, a significant number of organic moieties can be readily introduced onto the DPP-based π-conjugated framework to tune the photophysical properties. Besides, DPP derivatives have an inherent advantage of high molar extinction coefficient, and intensive NIR absorption and fluorescence emission, which endow them with great potential in optical imaging-guided tumor phototherapy [44].

With the malignant development of tumor cells, the tumor microenvironment (TME) will be formed, including not only the tumor cells, but also fibroblast, immune cells, inflammatory cells, glial cells, microvascular and related biomolecules [45]. With the continuous glycolysis process for tumor cells' energy supply, a large number of protons and carbon dioxide are generated within TME. In addition, many microvascular can be found for the tumor cells to survive in this hypoxic TME. Thus, the features for TME include hypoxia, weak acidity, and high glutathione (GSH)/ROS concentration. Especially, hypoxia is the Achilles' Heel for PDT, which has impeded the photodynamic effect in clinical [46]. And the weak acidity and high concentration of GSH/ROS have been employed as the target or trigger to enhance the phototherapeutic efficacy [47,48].

In this review, we will retrospect the DPP-based organic small molecular dyes for tumor phototheranostics. Firstly, we will summarize common design principles and synthetic routes for the DPP-derived dyes and the general preparation approaches for the corresponding multifunctional nanoplatform. Owing to the reactive sites of the DPP core, the DPP-derived dye molecules can be engineered through side-chain engineering and π-conjugation engineering. The relationship between their molecular structures and tumor diagnostic properties is highlighted, and finally, their future challenges and development prospects are discussed.

2. Preparation method

2.1. Synthesis of DPP-derived small molecular dyes

Generally, it is the first step to prepare an aryl-DPP (**1**) to construct functional DPP-derived small molecular dyes, while it is not easy to build the DPP core without the aryl group directly. And the condensation reaction between the aryl nitrile (Ar-CN) and succinate ester is the most common method to synthesis **1** with a yield of around 60%-80%, demonstrating the advantages of the wide availability of raw materials and high synthetic yield (Fig. 2) [49,50]. In addition, to synthesis **1**, tertiary alcohol salts are utilized as the base, and tertiary alcohols are often as solvents. This

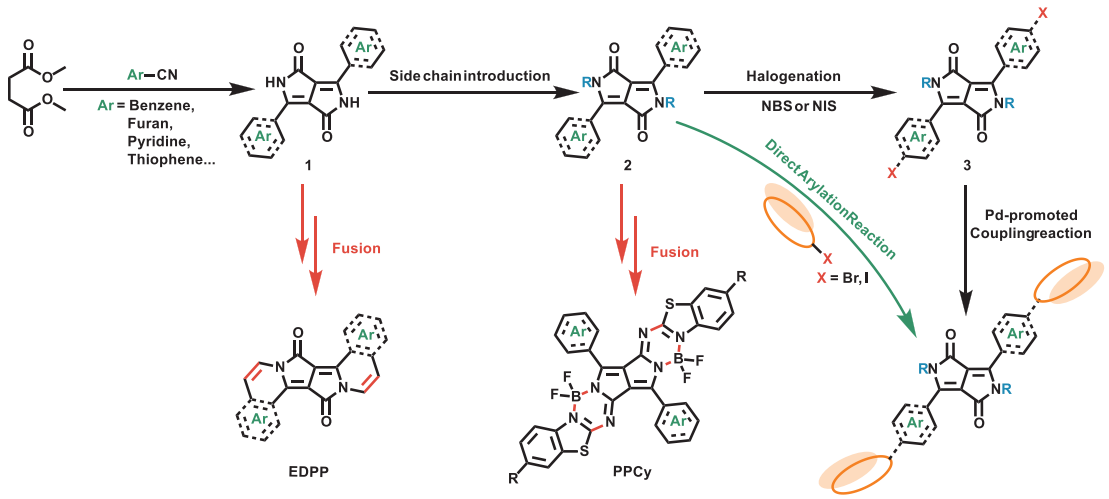

Fig. 2. Typical synthetic routes for various DPP-derived small molecular dyes.

is because the leaving group's excellent stability (alkoxyl anion) will facilitate the electrophilic reaction of the cyano unit. High synthetic yield is usually obtained from Ar-CN with low steric hindrance, especially electron-deficient Ar-CN. Electron-rich or spatially hindered aryl nitrile has low reactivity and low synthetic yields. And the most common reactant Ar-CN are 2-cyanofuran, 2-cyanothiophene, and 2-cyanoselenophene [51].

The second step is to introduce the side chain onto DPP to prepare **2**, improving the solubility and subsequent processability [44]. Hydrophobic or hydrophilic chains can be readily introduced. In most cases, hydrophobic alkyl hydrocarbon chains are installed as the side chain by taking *N,N*-dimethylformamide (DMF), or tetrahydrofuran (THF) are usually used as the solvent, and potassium carbonate is generally taken as the base. Hydrophilic side chains are typically introduced onto through further reaction with the terminal functional group, such as brominated alkyl chain.

To further extend the π-conjugation, Pd-catalyzed cross-coupling reaction, Pd-promoted direct arylation reaction, and ring-fusion can be commonly employed [52,53]. To employ Pd-catalyzed cross-coupling reactions, **1** is halogenated first with *N*-bromosuccinimide (NBS) or *N*-iodosuccinimide (NIS), then reacted with the organic boronic agent *via* Suzuki coupling reaction or reacted with the organic tin agent *via* Stille coupling reaction. Sometimes, the halogen atoms are included in the aryl-CN raw material for the synthesis of **1**. Brominated or iodinated π-conjugated units can also react with **1** directly *via* Pd-promoted direct arylation reaction to extend the π-conjugation. Ring-fusing strategy is a practical approach to prolong the π-conjugation length, and the lactam moiety with –C=O and –NH– units is the focus for ring-fusion to achieve a sizeable π-conjugated framework.

2.2. Preparation of the multifunctional nanoplatforms

Most organic dyes are insoluble in water, which means that the hydrophobic organic molecules will form aggregates, and cannot be delivered to the tumor site *via* blood circulation [54]. However, with the fast development of nanotechnology, it is promising to encapsulate the hydrophobic organic dyes into the amphiphilic polymers or proteins to fabricate the water-soluble organic nanoparticles as the theranostic nanoplatform. Therefore, by taking advantage of the enhanced permeability and retention (EPR) effect, the nanoparticles can efficiently accumulate at the tumor site [55].

At present, there are mainly three methods to prepare the water-soluble, (i) to introduce hydrophilic side chain, such as triethylene glycol chains, hyaluronic acid, to the DPP core; thus, the DPP-derivatives can form water-dispersible micelles as phototheranostic agents (Table 1) [56]. (ii) To employ amphiphilic polymers, such as Pluronic^{TM} F-127, DSPE-mPEG$_{2k}$, DSPE-mPEG$_{5k}$, lecithin, to encapsulate the DPP-derivatives through self-assembly for the preparation of biocompatible nanoparticles [57,58]. (iii) To rapidly inject a miscible organic solution containing DPP-derivatives into a large amount of deionized water under ultra-sonic to fabricate the discrete nanoparticles.

3. Molecular engineering of DPP-derived organic dyes for tumor theranostics

The typical DPP-derived functional dyes usually consist of three parts, the central DPP core, the side-chain groups, the π-bridge unit, and the terminal π-conjugated moieties. The side-chain groups can play a vital role in the solubility of the DPP derivatives. In comparison, the π-bridge units and the terminal π-conjugated moieties endow the DPP derivatives with various optoelectronic properties, which is of great importance for tumor phototheranostics.

3.1. Side-chain engineering

After the preparation of **1** with bad solubility, hydrophobic or hydrophilic side chains are introduced to improve the solubility for further purification and functionalization. In most cases, the hydrophobic alkyl hydrocarbon chains, such as 2-ethylhexyl and octyl groups, are introduced onto the DPP core through *N*-alkylation. However, some *O*-alkylated DPP derivatives can also be observed and separated [59]. Furthermore, hydrophilic side chains can also be introduced onto the DPP unit; thus, molecular micelles or functional NPs can be obtained. Additionally, with functional groups at the terminal site of the alkyl chains, the DDP derivatives can be further modified for multi-functionalization.

3.1.1. Introduction of hyaluronic acid as the side-chain

The clearance rate of most nanodrug is as high as 90% due to the lack of tumor-targeting ability. Therefore, it is urgent to design phototheranostic dyes that can efficaciously target tumor tissues. With cancer development, essential cytokines, such as IL-6, IL-10, TGF-β, and MMP, can be accumulated in the TME. Synchronously, there is an overexpression of some cellular products. These substances that are expressed abnormally in tumor sites can be used to target the tumor cells [60]. As an indispensable compound in

Table 1
Photophysical properties for the DPP-derived small molecular dyes for phototheranostics.

Therapeutic agent	Therapy mode	Imaging mode	Photophysical properties							Ref.
			Size [a] (nm)	λ_{abs}^{max} [b] (nm)	λ_{em}^{max} [b] (nm)	ε ($\times 10^4$ L mol^{-1} cm^{-1})	Φ_{Fl} [c]	Φ_{Δ} [d]	η [e]	
PDBr	PDT/PTT	FLI/PAI	~100	635	676	-	-	67%	35.7%	[51]
DTDPPBr2	PDT	-	-	560	589	-	-	16.2%	-	[62]
DTDPP-HA	PDT	-	-	534	565	-	-	12.8%	-	[63]
FDPP-HA	PDT	FLI	-	554	570	-	-	26%	-	[64]
DPP-Cb	PDT/PTT/CT	-	60	560	-	-	-	–	-	[67]
DPP-ATRA	PDT/PTT/CT	-	70	560	-	-	-	–	-	[67]
DPP-thiophene-4	-	FLI	~80 (pH 6.8)	543*	569*	-	-	-	-	[68]
DPP-TPA	PDT/PTT	PAI	~76	630	-	-	-	33.6%	34.5%	[73]
SeDPP-TPA	PDT/PTT	PAI	< 100	648	-	-	-	40.2%	37.9%	[74]
FDPP-TPA	PDT/PTT	FLI/PAI	123 ± 2	560	660	2.13 ± 0.2	–	40%	47%	[75]
TDPP	PDT	-	-	560*	610*	-	-	-	-	[76]
DPPCN-Fc	PTT	PAI	80 ± 2.3	728	-	3.03 ± 0.2	-	-	59.1%	[79]
DPP-TI	PDT/PTT	FLI	100 ± 18	633	663	-	-	48.3%	15.8 %	[80]
TDPP-Z	PTT	FLI/PTI	~125.6	645	636	-	-	-	20%	[81]
ThDPP-Au	PDT/PTT	FLI/PTI	~60	628	603	4.382	-	~65%	37.3%	[82]
Por-DPP	PTT	PAI	~120	745	-	-	-	-	62.5%	[83]
DPPBDPI	PDT	FLI	< 100	535	568	-	5%	80%	-	[84]
BD	-	FLI	~58	505	623	10.3	57%	-	-	[85]
BDB	-	FLI	~76	505	637	13.6	45%	-	-	[85]
DPP-BDT	PDT/PTT	FLI/PAI	~90	625*	980	3.35	0.52%	49.3%	23%	[86]
BDT(DPPCN)$_2$	-	FLI	~60.6	648	705	-	-	-	-	[87]
DPP-BT	PDT/PTT/CT	NIR-II FLI/PAI	~60	686*	1089*	3.05	-	27.3%	50%	[88]
PPAB	PTT	FLI/PAI	90 ± 7	698*	750*	-	-	-	47%	[89]
EDPP-6	-	-	-	654	663	1.99	84%	-	-	[90]
DPPTPh	PDT/PTT	FLI	58-192	612	651	-	-	22.3%	45.2%	[91]
DAA	PDT/PTT/CT	-	55 ± 2	650	-	1.91	-	39.7%	48.6%	[92]
DPP- NF	PDT/PTT/GT	-	60-70	623*	692*	-	-	-	45.6%	[93]
DPP-CD	PDT	-	10	530 (CDs)	-	-	-	27.6%	-	[94]

[a] The results were determined by DLS except for SeDPP-TPA.
[b] The spectral results were measured in the organic solvent, except for those marked with an asterisk (*) which were in the nanoparticle form.
[c] Fluorescence quantum yield.
[d] Singlet oxygen quantum yield.
[e] The photothermal conversion efficiency (η) was measured in the nanoparticle form.

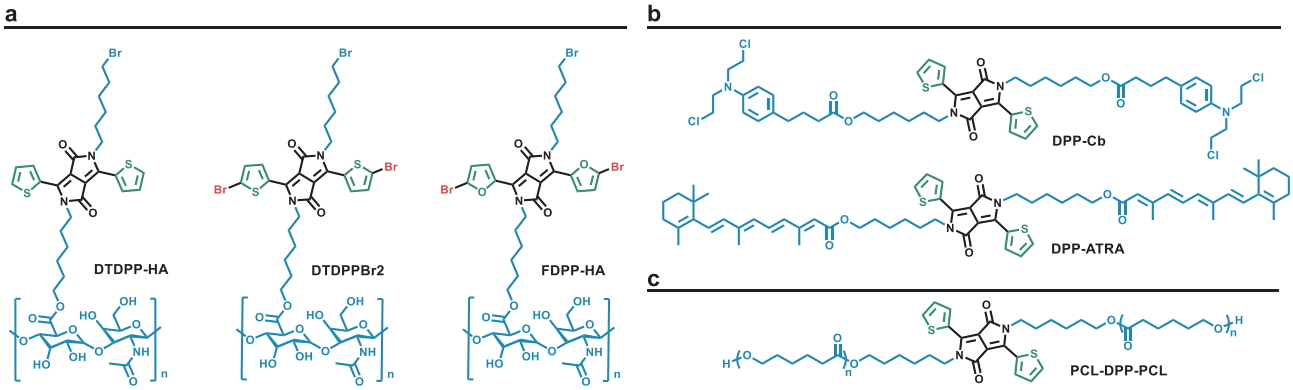

Fig. 3. Side-chain engineering of DPP-derived dyes. (a) Introduction of hyaluronic acid (HA) for tumor-targeting and solubilization; (b) Introduction of chemotherapeutic drugs for controlled release; (c) Introduction of polycaprolactone (PCL) as the side-chain.

the human body, hyaluronic acid (HA) is not only biocompatible and biodegradable but can also target CD44 specifically [61]. CD44 is involved in recirculation, homing, and other physiological cell processes as a kind of cell surface glycoprotein. Furthermore, it is overexpressed in specific cancer cells [62]. Hence, theranostic photosensitizers can gain the ability to target CD44-overexpressed cancer cells through HA modification.

A series of HA-modified DPP derivatives with good tumor-targeting performance and high reactive oxygen species generation efficiency have been reported. The HA side-chain is applied as the CD44 receptor to target the CD44-overexpressed cancer cells in these works. Dong *et al.* reported the HA-substituted thienyl-DPP photosensitizer DTDPP-HA, which exhibited a high $^1O_2$ quantum yield of 12.8% (Fig. 3a, Table 1) [63]. More remarkable, both *in vitro* and *in vivo* experiments revealed that DTDPP-HA could suppress tumor growth efficaciously. Therefore, DTDPP-HA would be a potential and promising phototheranostic agent.

Furthermore, Dong's group synthesized the photosensitizer DTDPPBr2 with two bromine atoms attached at the thiophene donors. With the introduction of the bromine atom, the intersystem crossing (ISC) efficiency could be improved by the heavy atom effect (Fig. 3a) [62]. Besides that, they also replaced the thiophene with furan as a donor group to obtain photosensitizer FDPP-HA, which increased the $^1O_2$ quantum yield to ~26% [64]. Remarkably, the HA-modifying strategy has also been applied in other photosensitizers design for cancer theranostics [65].

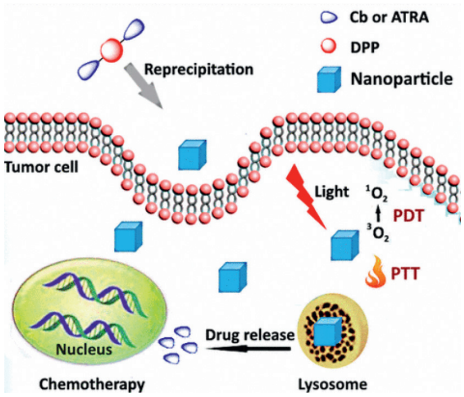

Fig. 4. Synergistic phototherapy and chemotherapy of DPP-Cb NPs and DPP-ATRA NPs based on pH-induced cleavage strategy. Copied with permission [67]. Copyright 2017, American Chemical Society.

3.1.2. Introduction of pH-responsive side-chains

With the malignant growth and high glycolytic process of tumor cells, many acidic metabolites, such as protons and carbon dioxide, are produced. Therefore, an acidic pH value of 6.5-6.8 results in tumor cells compared to 7.35-7.45 in normal cells [66]. At present, the weak acidity of the tumor microenvironment is regarded as a hallmark for solid tumors, and it has been widely utilized as a trigger for the design of pH-responsive nanotheranostic platforms. Several strategies, such as pH-induced cleavage and pH-induced protonation, have been developed now by researchers.

Carboxylic ester is a functional unit that can be cleaved through pH stimulus, and it has been introduced into the side-chain for controllable drug release to enhance chemotherapeutic efficacy. The carboxylic acid-containing chemotherapy drug, chlorambucil (Cb), and all-*trans*-retinoic acid (ATRA), were covalently conjugated onto the side-chains of DPP *via* carboxylic ester bond to prepare the photosensitizers DPP-Cb and DPP-ATRA (Figs. 3b and 4) [67]. The corresponding DPP-Cb NPs and DPP-ATRA NPs were prepared through the precipitation method. They exhibited a hydrodynamic size of around 60 nm, which was suitable for efficient accumulation at the tumor site of both NPs through the EPR effect. Under the acidic tumor microenvironment, the carboxylic ester bond would be readily cleaved to release the chemotherapeutic drug chlorambucil (Cb) or all-*trans*-retinoic acid (ATRA), which could enhance chemotherapy and reduce the side effect. Furthermore, *in vivo* experiments revealed that DPP-Cb NPs and DPP-ATRA NPs with good photothermal and photodynamic activity could accomplish synergistic PTT/PDT/chemotherapy to inhibit the tumor growth on HeLa tumor-bearing mice.

In addition, based on the pH-induced cleavage strategy, a small molecular amphiphilic dye DPP-thiophene-4 was innovatively designed and prepared with two alkyl side chains terminated with quaternary ammonium groups (Fig. 5, Table 1) [68]. With the help of the periphery hydrophilic quaternary ammonium units and hydrophobic thienyl-DPP core, DPP-thiophene-4 could achieve a nonfluorescent nanoassembly through self-assembly when pH was over 7.0; However, the nanoassembly could reversibly disassemble to fluorescent DPP-thiophene-4 monomers when pH was lower than 6.8. It is of great significance to note that the fluorescence emission signals exhibited a 10-fold enhancement within only a 0.2 pH unit change from pH 7.0 to pH 6.8, which could be employed to distinguish the malignant tumors among the healthy tissues *in vivo* owing to the weak acidity of the tumor microenvironment. The "off-on" fluorescence mechanism of DPP-thiophene-4 in water upon pH change was studied as well. A careful comparison of ^{1}H NMR spectra obtained at pH 6.8 and 7.0 implied that the protonation site was on the lactam N. DPP-thiophene-4 molecules could exist as either soluble monomers at pH 6.8 or aggregated nanoassemblies at pH 7.0. Therefore, its supramolecular self-assembly would subsequently take place once the deprotonation of DPP-thiophene-4 monomers along with pH 6.8 was switched to 7.0.

3.1.3. Introduction of polycaprolactone (PCL) as the side-chain

Polycaprolactone (PCL) is a nontoxic synthetic polyester chain widely applied for biomedical applications due to its excellent biocompatibility and biodegradability. It has attracted broad research interest in implantable biomaterials for tissue engineering and long-term drug delivery. DPP-derived polymer PCL-DPP-PCL was easily prepared through reaction with ε-caprolactone (Fig. 3c) [69]. Through nanoprecipitation with amphiphilic polymeric Pluronic® F-127, PCL-DPP-PCL NPs could be fabricated with high fluorescence quantum yield of 0.29 and excellent photostability, which was further applied for long-term fluorescence imaging.

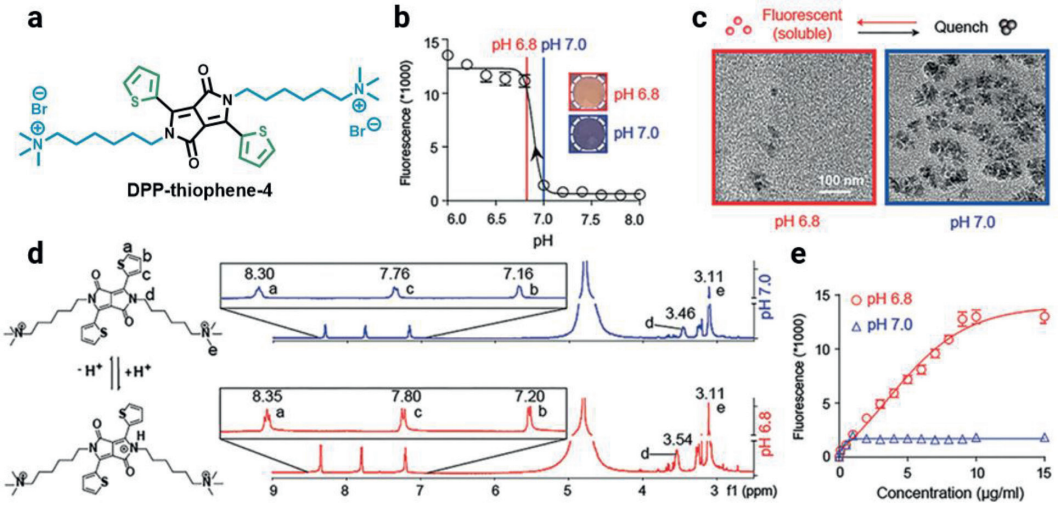

Fig. 5. A small molecular amphiphilic dye DPP-thiophene-4 based on the pH-induced decomposition strategy. (a) Chemical structure of DPP-thiophene-4; (b) The fluorescence intensity of DPP-thiophene-4 under various pH solutions; (c) The TEM images of DPP-thiophene-4 at either pH 6.8 or 7.0; (d) ^{1}H NMR results of DPP-thiophene-4 molecule between pH 6.8 and 7.0; (e) DPP-thiophene-4 solutions with different concentrations are prepared at either pH 6.8 or 7.0. Reproduced with permission [68]. Copyright 2017, American Chemical Society.

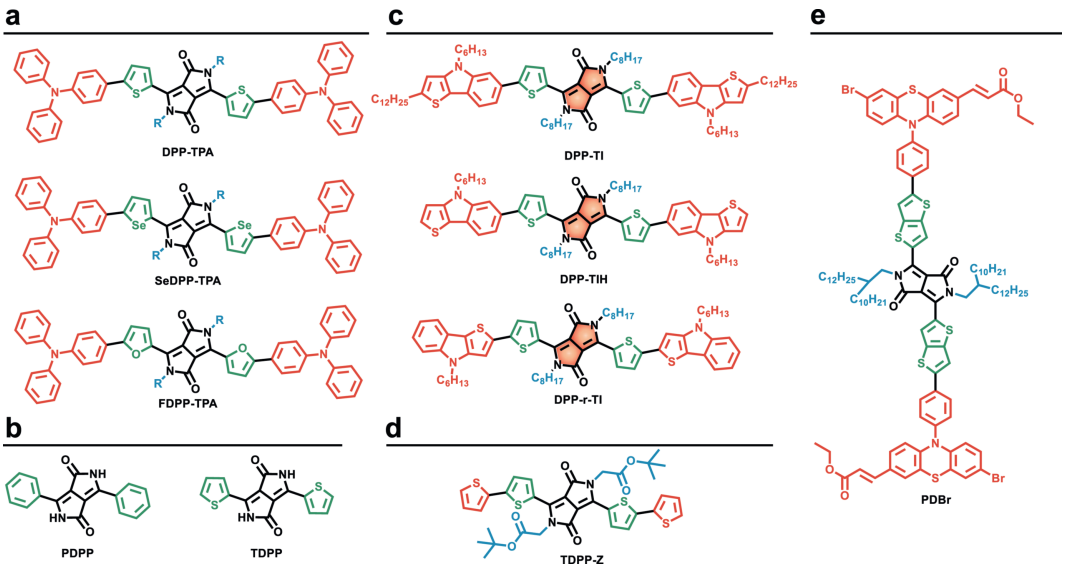

Fig. 6. π-Conjugation engineering of DPP-based photosensitizers. (a) Thiophene, selenophene and furan bridged DPP-based photosensitizers. (b) Phenyl and thienyl substituted DPP. (c) Chemical structures of DPP-TI, DPP-TIH, and DPP-r-TI. (d) Chemical structure of bisbithiophenyl-DPP photosensitizer TDPP-Z. (e) Chemical structure of PDBr.

3.2. π-Conjugation engineering

Phototheranostics include optical imaging and phototherapy, which are highly dependent on the photophysical processes, such as radiative decay, non-radiative decay, and intersystem crossing (ISC). As far as DPP-based theranostic photosensitizers, photophysical properties are dominated by the π-conjugated system. Especially, $^1O_2$ quantum yield and photothermal conversion efficiency, the two critical parameters of the phototheranostic agents for PDT and PTT, are profoundly influenced by the design of the π-conjugated DPP derivatives, which usually contains the central DPP core, π-bridges, and peripheral π-conjugated units. Due to the inherent electron-deficient nature of the DPP-core, the peripheral π-conjugated units are usually electron-rich groups. As is good to build D-A-D structures and facilitate the efficient intramolecular charge transfer (ICT) for red-shifted absorption/emission [70–72].

3.2.1. Effects of π-bridges

Within the D-π-A system, the introduction of the π-bridges can not only improve the intramolecular charge transfer (ICT), but also tune the molecular HOMO/LUMO energy levels. As the synthetic methodology for aryl-DPP derivatives mentioned in the previous part, the aryl unit is usually employed as the π-bridge, such as phenyl, thienyl, and furanyl unit (Fig. 6).

A series of DPP-derived photosensitizers DPP-TPA, SeDPP-TPA, and FDPP-TPA have been prepared with the same skeleton but different π-bridges (Fig. 6a) [73–75]. Through changing the π-bridges from thiophene to selenophene and furan, the maximum absorption peak changes from 630 nm to 648 nm, and 642 nm (in dichloromethane). In addition, DPP-TPA NPs present high photothermal conversion efficiency of 34.5%, while the photothermal conversion efficiency of SeDPP-TPA NPs and FDPP-TPA NPs were 37.9% and 47.0%, respectively. This implies that the introduction of furan and selenophene bridges enhanced the non-radiative transition. In contrast, the $^1O_2$ quantum yield was 33.6%, 40.2%, and 40% for DPP-TPA, SeDPP-TPA, and FDPP-TPA, respectively.

In addition, the theoretical energy gap between singlet state and triplet state (ΔE_{ST}) for phenyl and thienyl substituted DPP photosensitizers PDPP and TDPP (Fig. 6b) was 0.48 eV and 0.66 eV, respectively. It is indicated that TDPP could generate ROS more efficiently than PDPP, which was in accordance with the experimental results [76].

3.2.2. Effects of π-conjugated periphery units

Due to the high reactivity and easy functionalization of the α-position of the thiophene unit, thienyl-DPP is one of the most popular building blocks for the construction of multifunctional dyes. With subsequent bromination or iodination of the α-position of thiophene moiety, a significant number of functional dyes have been prepared through palladium-catalyzed coupling reactions or direct arylation reactions.

Through $Pd(OAc)_2$ catalyzed direct arylation reaction of thienyl-DPP, Dong's group prepared a D-A-D structured small molecular dye DPP-TPA for photoacoustic imaging-guided synergistic PDT/PTT [73]. After the introduction of the electron-donating triphenylamine (TPA) unit, intramolecular charge transfer (ICT) of DPP-TPA was enhanced to afford the bathochromic red-shift of the UV-vis absorption. However, the fluorescence emission and fluorescence lifetime were significantly decreased of the DPP and TPA segments after the covalent conjugation of DPP-TPA. Thus, the enhanced absorption and reduced fluorescence resulted in the good photothermal effect of DPP-TPA, which was beneficial to photoacoustic imaging, and DPP-TPA NPs could effectively hinder tumor growth through synergistic PDT/PTT upon 660 nm photoirradiation of living mice.

Ferrocene (Fc) with sandwich structure is a cancer therapeutic agent [77,78]. Liang *et al.* prepared a DPP derivative DPPCN-Fc by employing the Ferrocene unit as the periphery electron-rich unit (Fig. 7a, Table 1) [79]. In addition, an electron-deficient tetracyanobutadiene (TCBD) unit is introduced into the π-conjugated framework to build the D-A-D scaffold, which will result in an efficient ICT and bathochromic-shift absorption and promote the photo-induced electron transfer (PET) process. Therefore, after excitation of DPPCN-Fc, a charge transfer state was generated, and the radiative decay and intersystem crossing decay were quenched to give rise to heat. Thus, the photothermal conversion efficiency for DPPCN-Fc NPs was up to 59.1%, and DPPCN-Fc NPs demonstrated great cancer theranostic performance of photoacoustic imaging-guided tumor PTT without causing any side effect on living mice.

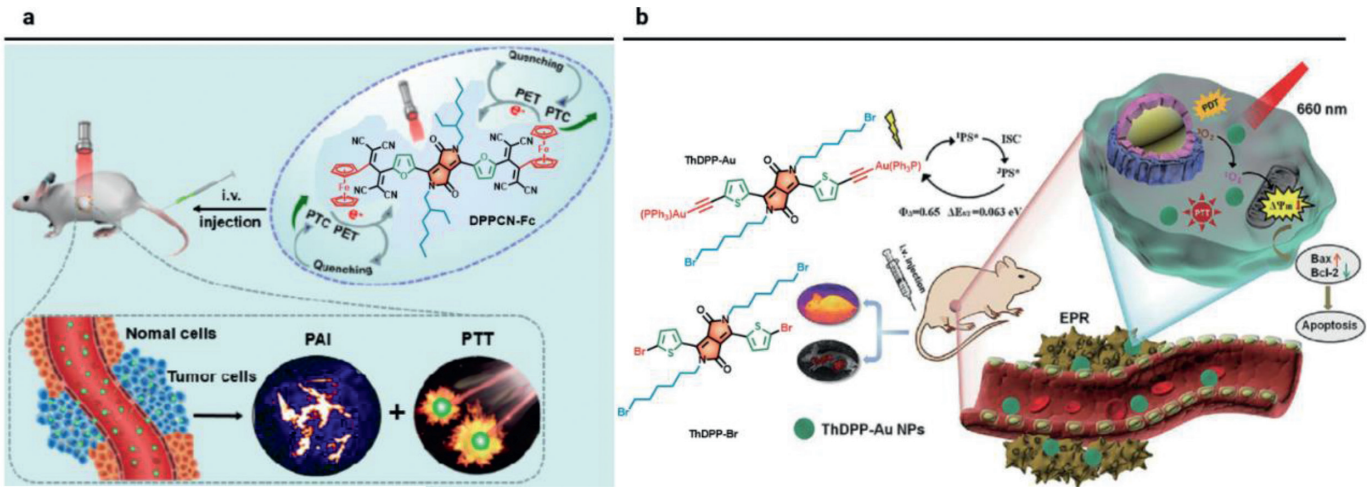

Fig. 7. Effects of π-conjugated periphery units. (a) The ferrocene unit functions as a donor group to quench fluorescence and generate $^1O_2$. Reproduced with permission [79]. Copyright 2017, Royal Society of Chemistry. (b) Heavy and gold atoms are introduced into phototherapeutic agents. Reproduced with permission [83]. Copyright 2019, Elsevier.

Thieno[2,3-*b*]indole (TI) is an electron-rich unit with a thiophene ring fused to the indole unit, and it has been used as a donor unit to conjugate with DPP for the preparation of photosensitizers DPP-TI, DPP-TIH, and DPP-r-TI (Fig. 6c) [80]. Since the three photosensitizers have the same DPP core, the maximum absorption wavelength is at 633, 626, and 661 nm (in toluene), respectively, which is significantly influenced by the donor moieties. And the optical bandgaps were 2.13 eV for DPP-TI, 2.15 eV for DPP-TIH, and 1.94 eV for DPP-r-TI. However, they showed a significant difference in the $^1O_2$ quantum yield, which was 48.3%, 0.3%, and 11.5% for DPP-TI, DPP-TIH, and DPP-r-TI, respectively. Thus, DPP-TI NPs were further prepared with a fluorescence lifetime of 2.3 ns and an excellent photothermal conversion efficiency of 15.8%. *In vitro* experiments demonstrated great potency for PDT/PTT.

In addition, the thiophene unit is also applied as the electron donor. And a bisbithiophenyl-DPP photosensitizer TDPP-Z was developed with a D-A-D motif (Fig. 6d) [81]. Upon 638 nm laser irradiation, TDPP-Z NPs presented an excellent photothermal conversion efficiency of 20%. However, owing to the aggregation-caused quenching (ACQ) effect, very weak fluorescence could be observed. *In vitro* and *in vivo* experiments showed that TDPP-Z NPs could realize fluorescence and photothermal imaging-guided PTT.

Atoms with a high atomic number, such as halogen atoms, are usually introduced into the π-conjugated molecules to improve ISC efficiency and facilitate the triplet state generation, as is known as the heavy atom effect. In general, the ISC rate (K_{ISC}) of the photosensitizer shows the dependency of the atomic number of halogen substituents (K_{ISC}~Z^4). For DPP-derived photosensitizers, bromine and iodine atoms are usually introduced to enhance ROS generation through the heavy atom effect (Fig. 6e).

As shown in Fig. 3a, DTDPP-HA and DTDPPBr2 with the only difference of two Br atoms on the π-conjugated periphery units of the latter were prepared by Dong's group [62,63]. The $^1O_2$ quantum yield was 12.8% for DTDPP-HA and 16.2% for DTDPPBr2. Although there is only a little enhancement of $^1O_2$ quantum yield for two bromo-substituted DTDPPBr2, it is an effective strategy towards the design of photosensitizer for PDT.

Heavy halogen atom substitution of photosensitizers still results in certain cytotoxicity. Therefore, developing a heavy halogen atom-free photosensitizer has attracted tremendous research interest [82]. To address this problem, triphenylphosphine-Au(I) was introduced into DPP-derived photosensitizer ThDPP-Au as a "spin converter" to facilitate the intersystem crossing for triplet state generation, and the singlet oxygen quantum yield was as high as 0.65 (Fig. 7b, Table 1) [83]. The theoretical calculation indicated that ThDPP-Au and its precursor ThDPP-Br exhibited significant intersystem crossing rate (K_{ISC}); However, the ratio of intersystem crossing rate to reverse intersystem crossing rate (K_{ISC}/K_{RISC}) for ThDPP-Au was higher than that of ThDPP-Br, suggesting that it was easier for the triplet ThDPP-Au to photosensitize oxygen for $^1O_2$ generation, not to go back to the singlet state. Under 660 nm laser irradiation, ThDPP-Au NPs exhibited an excellent photothermal conversion efficiency of 37%. *In vitro* experiments showed that ThDPP-Au NPs could effectively kill tumor cells through the $^1O_2$-induced mitochondrial apoptosis pathway. Guiding by dual fluorescence imaging and photothermal imaging, *in vivo* results on HeLa-tumor-bearing mice confirmed the significant anti-cancer effect of synergistic PDT/PTT. This work provides a new way towards the design of halogen-free photosensitizers for efficient phototherapy.

Near-infrared (NIR) optical imaging, including NIR-I (700-900 nm) and NIR-II (1000-1700 nm), is usually considered as the promising alternative to conventional optical imaging techniques, because of its deep tissue penetration, low tissue auto-fluorescence, high signal-to-noise ratio, and minimal photodamage [84]. The absorption wavelength of the common aryl-DPP is around ~500 nm, locating in the visible region. To achieve better optical imaging performance, it is necessary to push the absorption of the DPP-derived organic dyes more red-shifted. And there are three molecular design strategies commonly applied to synthesis the DPP derivatives with bathochromic shift, (i) extending the π-conjugation, (ii) constructing the D-A motif, and (iii) fusing the DPP unit with aromatic rings [85].

Till now, a lot of π-conjugated dyes or building blocks, such as porphyrin, boron dipyrromethane (BODIPY), and benzodithiophene (BDT), have been employed to covalently bond with the DPP core for multi-functionalization. Porphyrin derivatives of PpIX (protoporphyrin IX) and HPD (hematoporphyrin derivative) are the first- and second-generation photosensitizers in clinical, and they can absorb visible light to generate $^1O_2$ for PDT. Taking into this consideration, Zhang *et al.* constructed a porphyrin-based amphiphilic NIR photosensitizer Por-DPP for tumor phototheranostics (Fig. 8a) [86]. In this triad structure, two DPP units as electron acceptors were conjugated with the central electron-donating porphyrin unit through the alkyne group. With two triethylene glycol flexible chains attached to the central porphyrin unit, water-soluble Por-DPP NPs were readily prepared through self-assembly, and

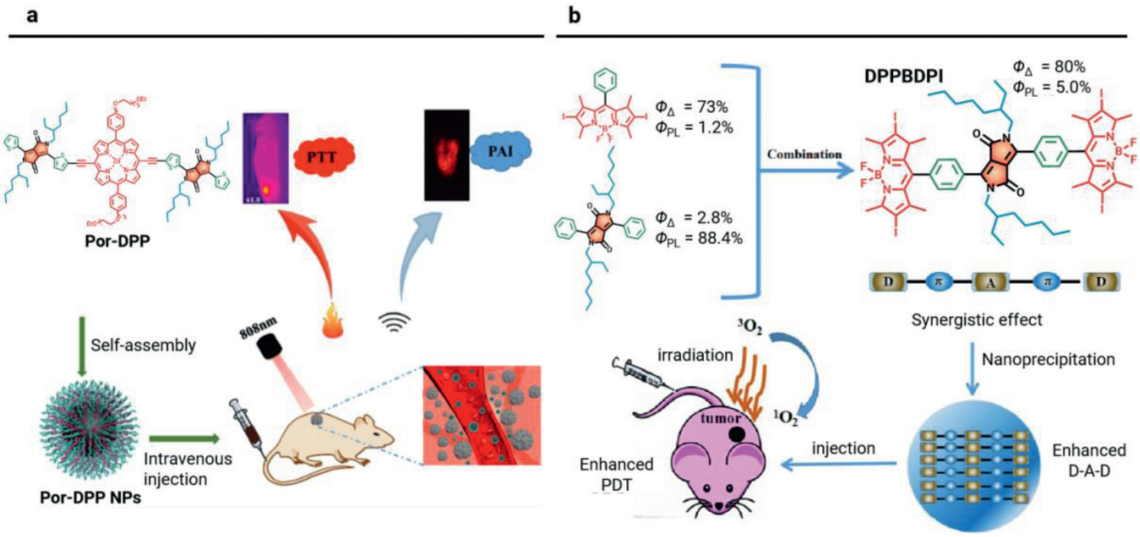

Fig. 8. (a) Porphyrin and DPP-based phototherapeutic agent Por-DPP for photoacoustic imaging-guided PTT. Reproduced with permission [86]. Copyright 2019, American Chemical Society. (b) BODIPY and DPP-derived photosensitizer DPPBDPI for fluorescence imaging-guided PDT. Reproduced with permission [88]. Copyright 2018, Royal Society of Chemistry.

exhibited a broad absorption profile with a significant bathochromic shift in water. Owing to the A-D-A motif of the triad, Por-DPP NPs with favorable non-radiative decay presented photothermal conversion efficiency of 62.5%. Thus, photoacoustic imaging-guided PTT was realized of Por-DPP NPs on HeLa tumor-bearing mice with great biocompatibility.

BODIPY is one of the essential organic dyes that has been widely used in biosensors and nanomedicine [87]. The BODIPY moiety is also attached to DPP core to build functional dyes for tumor phototheranostics. Dong's group designed a D-A-D structured triad DPPBDPI by taking DPP as the electron acceptor and BODIPY as the electron donor (Fig. 8b) [88]. DPPBDPI showed a simultaneous increase of the fluorescence QY of 5.0% and the $^1O_2$ quantum yield of around 80% with the synergistic combination of the two moieties. Through nanoprecipitation, DPPBDPI NPs were prepared to show fluorescence imaging-guided PDT on Hela-tumor-bearing mice. Additionally, two triads of BD and BDB containing DPP and BODIPY units were prepared for fluorescence imaging of Hela cells and zebrafish [89].

BDT (benzo[1,2-*b*:4,5-*b*']dithiophene) is an electron-rich unit that has been widely applied for organic photovoltaics and organic field-effect transistors [44]. Recently, a considerable amount of functional small molecular organic dyes combined DPP and BDT have also been constructed as phototherapeutic agents for cancer theranostics. Fan's group designed a NIR triad DPP–BDT with two flanked DPP moieties for combined PDT/PTT guided by dual-mode NIR-II fluorescence/photoacoustic imaging (Fig. 9a) [90]. DPP-BDT NPs showed the maximum absorption peak at 625 nm, and a broad fluorescence spectrum peaked at 980 nm. Significantly, the emission spectra went into the NIR-II region, indicating the enhanced depth and resolution of fluorescence imaging. Furthermore, the $^1O_2$ quantum yield of DPP-BDT NPs was 49.3%, and the photothermal conversion efficiency was 62.5%. The multifunctional DPP-BDT NPs required only a single wavelength laser of 660 nm for excitation to achieve dual-mode NIR-II fluorescence/photoacoustic imaging-guided PDT/PTT. This feature showed remarkable advantages for clinical applications. In addition, Stefan's group also designed a D-π-A structured small molecular dye BDT(DPPCN)$_2$ for fluorescence imaging (Fig. 9b) [91]. However, the triad BDT(DPPCN)$_2$ demonstrated a low fluorescence quantum yield of 0.25%, which could be attributed to the favored non-radiative attenuation induced by the numerous alkyl chains.

BT (2,1,3-benzothiadiazole) is a typical electron acceptor for organic electronics and biophotonics [92–94]. Fan's group put forward an innovative "all-in-one" strategy to develop a small molecular triad dye DPP-BT with emission from 900 nm to 1300 nm for NIR-II fluorescence and photoacoustic imaging-guided cancer therapy (Fig. 9c) [95]. The phototherapeutic platform based on DPP-BT was employed not only as a phototheranostic agent for NIR-II FLI/PAI-guided phototherapy but also as a carrier of chemotherapeutic drug DOX (doxorubicin) for chemotherapy. Additionally, P(DPP-BT/DOX) NPs showed a fluorescence quantum yield of 0.42%. After accumulation into tumor tissues, upon 730 nm photoirradiation, P(DPP-BT/DOX) NPs could release the chemotherapeutic DOX effectively for chemotherapy with the help of the photothermal effect. Additionally, fluorescence imaging and photoacoustic imaging could precisely locate the tumor and depict the tumor outline. Moreover, the cancers could be monitored in real-time for efficient PDT/PTT/chemotherapy with P(DPP-BT/DOX) NPs.

Fusing the DPP unit with aromatic rings to construct a sizeable π-conjugated framework is an effective method to push the absorption/emission spectra red-shifted. The lactam is the reactive site to fuse the aromatic rings. The carbonyl group in DPP can react with aryl-amine through a condensation reaction. Based on this, Wu *et al.* synthesized a polycyclic aromatic molecule PPAB by fusing DPP with aza-BODIPY unit (Fig. 10a) [96]. After expanding the π-conjugation, PPAB demonstrated an absorption maximum at 698 nm. PPAB NPs displayed an absorption peak at 752 nm and high photothermal conversion efficiency of 47%. Through tail vein administration on HeLa-tumor-bearing mice, PPAB NPs realized fluorescence/photoacoustic imaging-guided PTT with great biosafety. In addition, Kouichi *et al.* prepared a two-PEG-chains grafted NIR dye PPAB. The PEGlated PPAB showed an absorption peak at 752 nm but no fluorescence in water; thus, the photoacoustic imaging performance was studied, and PEGlated PPAB demonstrated stronger photoacoustic signals than that of ICG.

The carbonyl group can also react with electron-deficient methylene moiety *via* a condensation reaction. And Huang *et al.* employed 2-cyanomethylpyridine derivative to condensate with the DPP core for the preparation of the π-extending PPCy (pyrrolopyrrole cyanine) (Fig. 10b) [97]. Through further functionalization with bulky spirofluorene derivative, highly fluorescent dye PPCy-SF was prepared. Furthermore, PPCy-SF NPs presented an excellent *in vivo* fluorescence imaging performance.

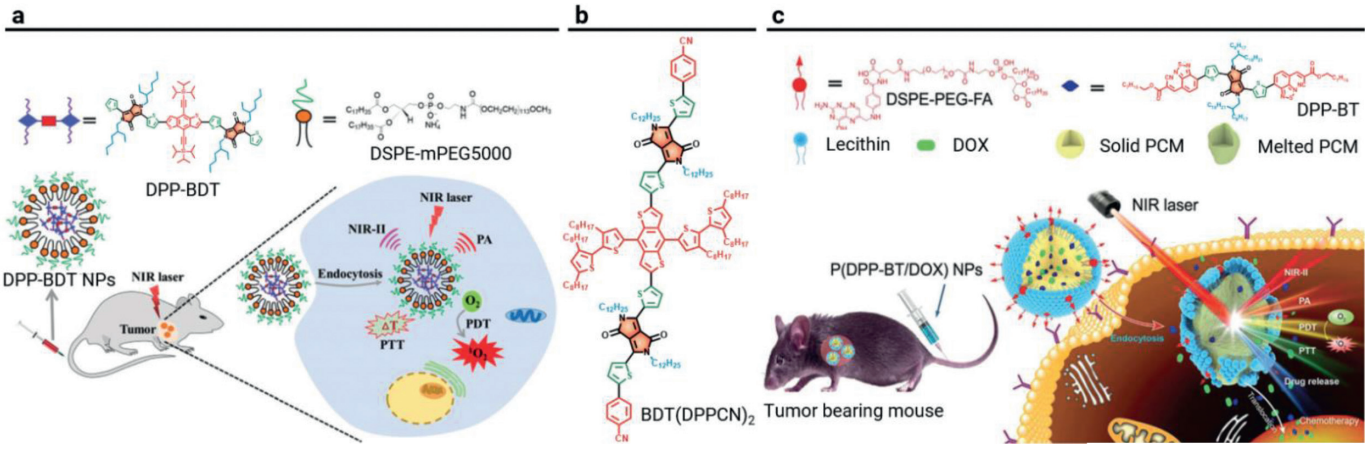

Fig. 9. "All-in-one" strategy in the design of DPP-based phototherapeutic agents. (a) PAI/FLI-guided PDT/PTT of DPP-BDT. Reproduced with permission [90]. Copyright 2019, Royal Society of Chemistry. (b) Chemical structure of small molecular dye BDT(DPPCN)2. (c) Phototheranostic P(DPP-BT/DOX) NPs for NIR-II fluorescence/photoacoustic imaging-guided PDT/PTT/chemotherapy. Reproduced with permission [95]. Copyright 2019, Wiley-VCH.

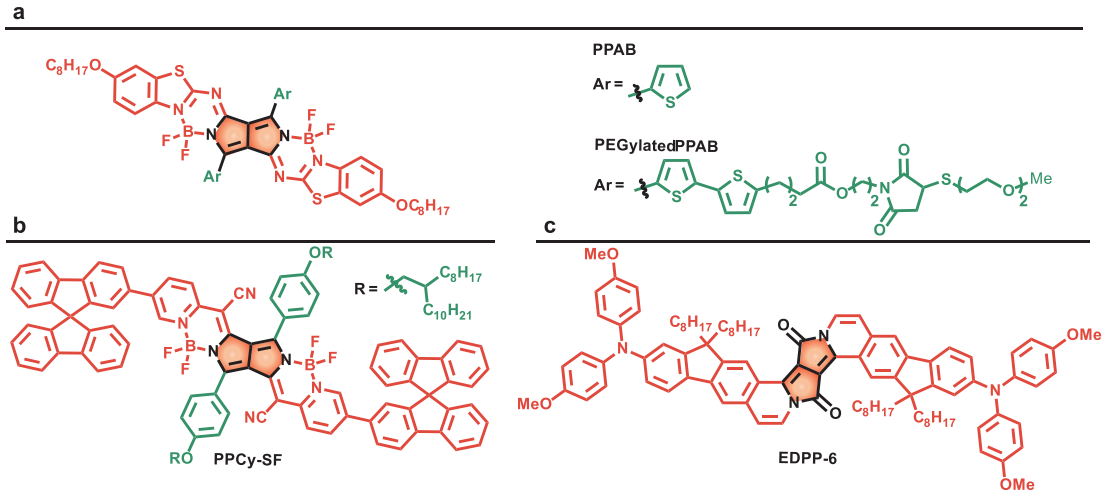

Fig. 10. Chemical structures of the fused π-conjugated dyes: (a) PPAB and PEGlated PPAB, (b) PPCy-SF, (c) EDPP-6.

In addition, the 2-cyanofluorene derivative can also be applied for the construction of the DPP core. And Grzybowski *et al.* prepared a series of fluorene-DPP and then introduced 2-bromoacetaldehyde diethyl acetal as the alkyl chain (Fig. 10c) [98]. Through subsequent acid-triggered aromatic cyclization, additional vinylene units were embedded to construct the polycyclic aromatic molecules EDPP. Two-photon absorption cross-section (δ_{2PA}) of EDPP-6 at 1050 nm was around 1410 GM in chloroform, demonstrating great potency for two-photon fluorescence imaging.

Stimulus-responsive photosensitizer can target interact with specific substance and induce corresponding "turn on" or "turn off" phenomenon, which can be utilized to enhance the phototherapeutic effect [99–101]. GSH is a featured bio-reductant in solid tumors, which presenting a 10-fold higher concentration in tumor cells than in normal cells [102,103]. GSH can react with oxidative ROS to impede PDT efficacy. Thus, GSH-responsive nanotheranostic agents have gained increasing attention to enhance therapeutic efficacy. 2,3,3-Triphenylacrylonitrile-containing photosensitizer DPPTPh with GSH-depletion reactivity was developed for fluorescence "turn on" imaging and enhanced PDT/PTT (Fig. 11) [104]. The Michael addition reaction between -SH group in GSH and the cyano- group in photosensitizer DPPTPh could generate thiazole unit, as would efficiently consume the intratumoral GSH for enhanced phototherapy and "turn-on" the fluorescence of DPPTPh for fluorescence imaging. In addition, under 660 nm photoirradiation, DPPTPh NPs displayed a photothermal conversion efficiency of 45.2% and a singlet oxygen quantum yield of 22.3%. *In vivo* studies showed that DPPTPh NPs could accomplish not only GSH-triggered fluorescence imaging but also synergistic PDT/PTT.

3.3. Multi-functionalization of side chain and π-conjugation units

Towards the design of DPP-based phototherapeutic agents, the side-chain engineering or π-conjugated system engineering strategy has been introduced previously; furthermore, the two approaches can be combined together for multi-functionalization. As a result, optical imaging-guided multi-modes cancer therapy can be readily accomplished.

During the tumor progression, vascular endothelial growth factor (VEGF) within the tumor microenvironment (TME) will be upregulated for new vasculature generation. Especially, free tumor cells or certain inducible factors will come into blood vasculature to circulate, which will result in metastasis. As a result, it is of great importance to develop anti-vascular therapy, not only to impede the nutrition and oxygen supply for limotherapy but also to prevent tumor metastasis [105,106].

Based on this, Liang *et al.* took advantage of the ester group to introduce the anti-vascular agent 5,6-dimethylxanthenone-4-acetic acid (DMXAA) to the side chain for the preparation of DPP-based phototherapeutic agent DAA (Fig. 12a) [107]. In addition, pH-

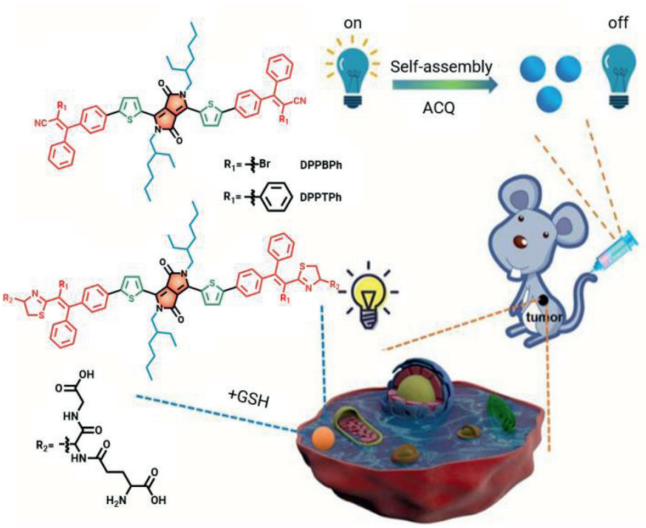

Fig. 11. Glutathione-responsive photosensitizer design, also used as glutathione probes. Reproduced with permission [104]. Copyright 2019, Royal Society of Chemistry.

responsive diethylaminophenyl (DEAP) units were also introduced at periphery sites of the thienyl-DPP to prolong the π-conjugation length for the construction of the D-A-D scaffold. Upon 660 nm laser irradiation, DAA NPs presented a high photothermal conversion efficiency of 48.6% (pH 7.4) and a good $^1O_2$ quantum yield of 39.7% (12.5 mmol/L trifluoroacetic acid). After DAA NPs efficient accumulation at the tumor site, anti-vascular DMXAA could be efficiently released from the phototherapeutic agent DAA through the weak acidity-promoted ester hydrolysis, thereafter to target vascular endothelial growth factor (VEGF) and effectively destroy vascular for anti-vascular therapy. In addition, under the acidic tumor microenvironment, the N atoms of DEAP were protonated. The photo-induced electron transfer (PET) process would be quenched to turn on the intersystem crossing channel for $^1O_2$ generation the radiative decay channel for fluorescence imaging. Simultaneously, the photothermal effect was enhanced after the protonation of the DEAP group. *In vitro* studies showed excellent anti-vascular performance on human umbilical vein endothelial cells (HUVECs). And *in vivo* studies demonstrated that DAA NPs could accomplish fluorescence imaging-guided synergistic anti-vascular therapy and photothermal/photodynamic therapy.

Many kinds of gas molecules, such as NO, CO, play essential roles as messenger molecules in the human body. In 1998, NO-mediated cardiovascular disease treatment was awarded Nobel Prize. From then on, gas therapy has attracted increasing research attention. Recently, gap therapy has been applied to combine with phototherapy to enhance the phototherapeutic efficacy [108]. Dong's group developed a nitric oxide (NO) donor-containing phototheranostic agent DPP-NF NPs for synergistic gap therapy and phototherapy (Figs. 12b and c) [109]. 4-Nitro-3-trifluoromethylaniline moiety was introduced into the side chain as the NO donor for photo-induced gas therapy. And dimethylaminophenyl units were flanked at the periphery sites of the DPP core for pH-enhanced PDT/PTT. The photothermal conversion efficiency of DPP-NF NPs was determined to be 45.6% under 660 nm laser irradiation. Upon photoirradiation of DPP-NF NPs, a photo-induced rearrangement from nitro- to nitrite- took place to generate NO radicals; While under dark, almost no nitric oxide could be produced by DPP-NF NPs. This controllable release behavior of DPP-NF NPs could overcome the drawback of excessive NO-release. Based on the HeLa-bearing mice model, DPP-NF NPs exhibited excellent fluorescence imaging-guided anti-tumor effect by the combination of gas therapy and pH-activated PDT/PTT.

3.4. DPP-based carbon dots as phototherapeutic agent

In recent years, carbon dots (CDs), a kind of *quasi*-0D carbon-based nanomaterials, are widely used in optical/energy devices and

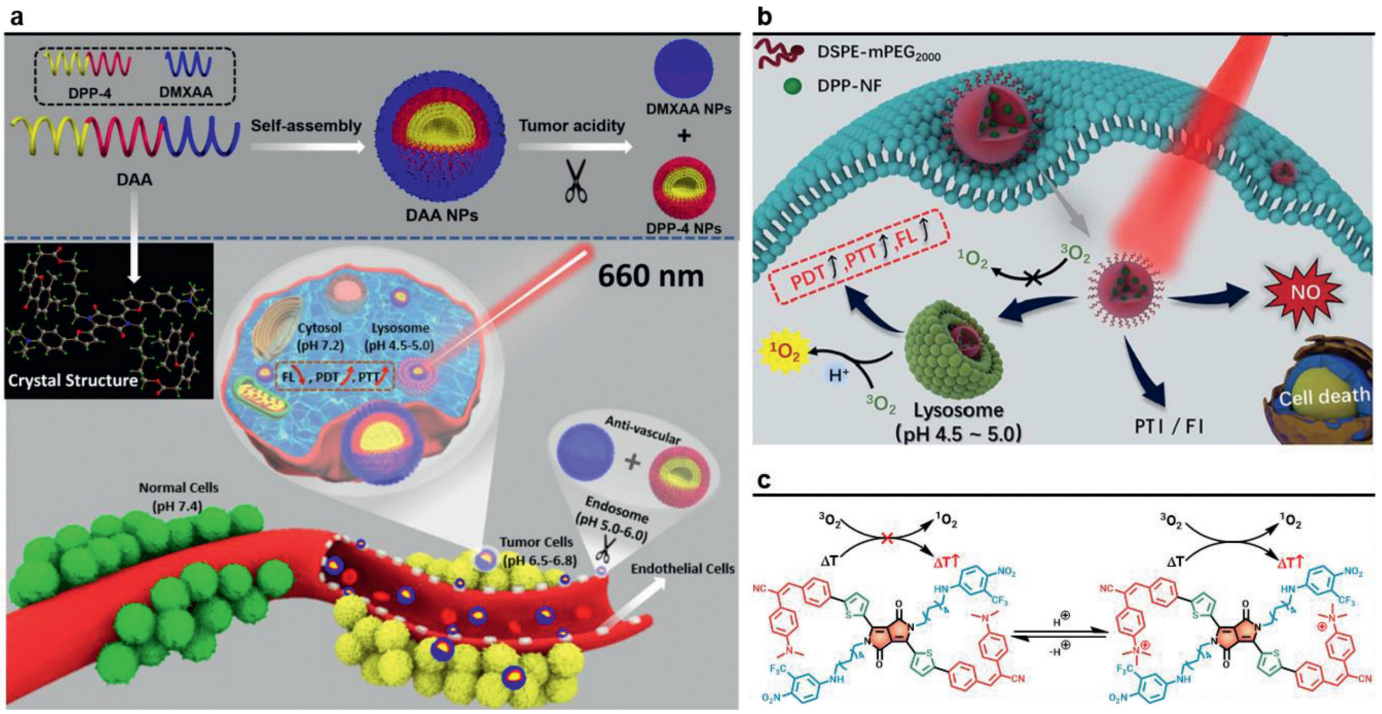

Fig. 12. Multi-functionalization of DPP. (a) **DAA** NPs with synergistic anti-vascular activity and pH-enhanced PDT/PTT. Copied with permission [107]. Copyright 2019, Royal Society of Chemistry. (b, c) pH-responsive **DPP-NF** NPs for gas therapy and pH-activated PDT/PTT. Reproduced with permission [109]. Copyright 2018, American Chemical Society.

nanomedicine, because of their excellent photostability, water solubility, and biocompatibility [110]. Fluorescent carbon dot DPP-CD based on DPP-derived small molecular dye and chitosan was developed through a simple one-pot hydrothermal method [111]. It not only maintained the capability of the DPP photosensitizer to produce $^1O_2$, but also possessed excellent hydrophilicity and biosafety. *In vitro* and *in vivo* experiments showed that DPP carbon dots effectively inhibited the growth of tumor cells under laser irradiation.

4. Conclusions and outlook

Herein, we have summarized recent advances towards the design and construction of DPP-based small molecular dyes for tumor phototheranostics. Owing to remarkable structural tunability, various side chains and peripheral π-conjugated units can be introduced to endow multi-functionalization. Hydrophilic side chains, such as hyaluronic acid (HA) can be introduced to form phototheranostic nanomicelles with good tumor-target performance. In addition, pH-responsive side chains can also be introduced to enable DPP photosensitizer as a chemotherapeutic drug carrier, thus accomplishing enhanced chemotherapy and phototherapy. Furthermore, to extend the π-conjugation of DPP derivatives, different building blocks, such as porphyrin, BODIPY, BDT, and BT, are employed to construct functional dyes and corresponding phototheranostic nanoplatform. Fusing the DPP unit to build polycyclic aromatic molecules can also be used for imaging-guided phototherapy. Last but not least, through modification of the side chain and the π-conjugated system, other therapeutic modes, such as gas therapy and anti-vascular therapy, can be combined with phototherapy.

With the abundant modification of the DPP core, many functional dyes have been synthesized as multifunctional anti-tumor phototheranostic nanoplatform. Nevertheless, there are still some challenges for the development and application of DPP-derived small molecular dyes. First, with the feature of easy structure tunability of DPP, it is of great superiority to develop DPP-derived small molecular dyes and finely tune the triplet states for type I PDT, which can overcome the hypoxia issue for traditional PDT. Second, many DPP-based small molecular dyes are now passively accumulated in the tumor tissues through the EPR effect. As a result, it is urgent to exploit small molecular DPP dyes with the active tumor-target property. In addition, to fully take advantage of the tumor microenvironment for enhanced phototherapeutic efficacy, it is of great significance to develop tumor microenvironment-responsive DPP dyes. Third, as-developed DPP-based small molecular dyes mainly work in the NIR-I biological window at present. To further exploit the application of DPP-based small molecular dyes for optical imaging and phototherapy, DPP-derived dyes with NIR-II absorption or fluorescence emission should be taken into consideration. Fourth, immunotherapy is a promising personalized anti-tumor approach. It is of great significance to develop multifunctional DPP-based dyes for combinational phototherapy and immunotherapy [112]. Furthermore, based on the “all-in-one” strategy, it is essential to integrate optical/acoustic/magnetic imaging modes and other therapeutic modes, such as chemodynamic therapy or gene therapy, into the multifunctional DPP dyes.

Declaration of competing interest

The authors declare that they have no known competing financial interests or personal relationships that could have appeared to influence the work reported in this paper.

Acknowledgments

This work was supported by the National Natural Science Foundation of China (No. 21972067), and the Natural Science Foundation of Jiangsu Province (Nos. BK20200092 and BK20200710). We are also grateful to the High-Performance Computing Center in Nanjing Tech University for supporting the computational resources.

References

[1] J. Ferlay, M. Colombet, I. Soerjomataram, et al., Int. J. Cancer 144 (2019) 1941–1953.
[2] X. Li, N. Kwon, T. Guo, et al., Angew. Chem. Int. Ed. 57 (2018) 11522–11531.
[3] C. Xie, X. Zhen, Q. Miao, et al., Adv. Mater. 30 (2018) 1801331.
[4] D. Chen, Z. Zhong, Q. Ma, et al., ACS Appl. Mater. Interfaces 12 (2020) 26914–26925.
[5] Z. Zhao, C. Chen, W. Wu, et al., Nat. Commun. 10 (2019) 768.
[6] X. Li, S. Lee, J. Yoon, Chem. Soc. Rev. 47 (2018) 1174–1188.
[7] Y. Cai, W. Si, W. Huang, et al., Small 14 (2018) 1704247.
[8] L. Li, Y.S. Chen, W.J. Chen, et al., Chin. Chem. Lett. 30 (2019) 1689–1703.
[9] W. Hu, P.N. Prasad, W. Huang, Acc. Chem. Res. 54 (2021) 697–706.
[10] Q. Yu, X. Huang, T. Zhang, et al., Chem. Res. Chin. Univ. 37 (2021) 951–959.
[11] Y. Wang, Y. Liu, H. Sun, D. Guo, Coord. Chem. Rev. 395 (2019) 46–62.
[12] X. Huang, X. Sun, W. Wang, et al., J. Mater. Chem. B 9 (2021) 3756–3777.
[13] D.P. Chen, Z.C. Wang, H.M. Dai, et al., Small Methods 4 (2020) 2000013.
[14] D. Chen, J. Zhang, Y. Tang, et al., J. Mater. Chem. B 6 (2018) 4522–4530.
[15] Y. Wang, W. Wu, J. Liu, et al., ACS Nano 13 (2019) 6879–6890.
[16] D. Chen, Q. Xu, W. Wang, et al., Small 17 (2021) 2006742.
[17] X. Zhen, P. Cheng, K. Pu, Small 15 (2019) 1804105.
[18] D. Chen, Q. Yu, X. Huang, et al., Small 16 (2020) 2001059.
[19] Z.J. Cheng, T. Zhang, W.L. Wang, et al., Chin. Chem. Lett. 32 (2021) 1580–1585.
[20] Y.S. Chen, L. Li, W.J. Chen, et al., Chin. Chem. Lett. 30 (2019) 1353–1360.
[21] S. Wang, W. Wu, P. Manghnani, et al., ACS Nano 13 (2019) 3095–3105.
[22] B. Guo, Z. Feng, D. Hu, et al., Adv. Mater. 31 (2019) 1902504.
[23] H. Dai, Q. Shen, J. Shao, et al., Innovation 2 (2021) 100082.
[24] L. Tu, Y. Xu, Q. Ouyang, et al., Chin. Chem. Lett. 30 (2019) 1731–1737.
[25] Z. Xie, T. Fan, J. An, et al., Chem. Soc. Rev. 49 (2020) 8065–8087.
[26] J. Zhang, J. Chen, J. Ren, et al., Biomaterials 181 (2018) 92–102.
[27] L. Huang, G. Han, Small Methods 2 (2018) 1700370.
[28] W. Xiao, P. Wang, C. Ou, et al., Biomaterials 183 (2018) 1–9.
[29] X. Yang, G. Liu, Y. Shi, et al., Nanotechnology 29 (2018) 222001.
[30] J. Li, K. Pu, Chem. Soc. Rev. 48 (2019) 38–71.
[31] B. Joseph, S.V.K.C. Sabu, et al., J. Bioresour. Bioprod. 5 (2020) 231–247.
[32] L. Cheng, C. Wang, L. Feng, et al., Chem. Rev. 114 (2014) 10869–10939.
[33] C.M. Ewulonu, X. Liu, M. Wu, H. Yong, J. Bioresour. Bioprod. 4 (2019) 3–10.
[34] R.F. Mendes, F. Figueira, J.P. Leite, et al., Chem. Soc. Rev. 49 (2020) 9121–9153.
[35] X. Huilin, Z. Dongyue, L. Jianshu, J. Bioresour. Bioprod. 4 (2019) 177–182.
[36] X. Zhen, C. Xie, K. Pu, Angew. Chem. Int. Ed. 57 (2018) 3938–3942.
[37] Y. Lyu, J. Zeng, Y. Jiang, et al., ACS Nano 12 (2018) 1801–1810.
[38] K. Ding, Y. Zhang, W. Si, et al., ACS Appl. Mater. Interfaces 10 (2018) 238–247.
[39] Y. Tang, L. Xue, Q. Yu, et al., ACS Appl. Bio Mater. 2 (2019) 5888–5897.
[40] X. Li, D. Lee, J. Huang, J. Yoon, Angew. Chem. Int. Ed. 57 (2018) 9885–9890.
[41] A. Kamkaew, S.H. Lim, H.B. Lee, et al., Chem. Soc. Rev. 42 (2013) 77–88.
[42] Y. Zhang, S. Bo, T. Feng, et al., Adv. Mater. 31 (2019) 1806444.
[43] Y. Patil, R. Misra, Chem. Rec. 20 (2020) 596–603.
[44] A. Tang, C. Zhan, J. Yao, E. Zhou, Adv. Mater. 29 (2017) 1600013.
[45] L. Feng, Z. Dong, D. Tao, et al., Natl. Sci. Rev. 5 (2018) 269–286.
[46] W. Fan, P. Huang, X. Chen, Chem. Soc. Rev. 45 (2016) 6488–6519.
[47] P. Zheng, Y. Liu, J. Chen, et al., Chin. Chem. Lett. 31 (2020) 1178–1182.
[48] D. Jia, X. Ma, Y. Lu, et al., Chin. Chem. Lett. 32 (2021) 162–167.
[49] Z. Hao, Chem. Soc. Rev. 26 (1997) 203.
[50] S. Qu, H. Tian, Chem. Commun. 48 (2012) 3039–3051.
[51] X. Yang, Q. Yu, N. Yang, et al., J. Mater. Chem. B 7 (2019) 2454–2462.
[52] J. Shao, G. Wang, K. Wang, et al., Polym. Chem. 6 (2015) 6836–6844.
[53] Z. Wang, Q. Ma, X. Huang, et al. , Chin. Chem. Lett. 33 (2022) 271–275.
[54] L. Cheng, Chem. Rev. 114 (2014) 10869.
[55] J. Ding, J. Chen, L. Gao, et al., Nano Today 29 (2019) 100800.
[56] J. Schmitt, V. Heitz, A. Sour, et al., Angew. Chem. Int. Ed. 54 (2015) 169–173.
[57] P. Wang, W. Wu, R. Gao, et al., ACS Appl. Mater. Interfaces 11 (2019) 13935–13944.
[58] Y. Cao, J.W. Yi, X. Yang, et al., Biomacromolecules 18 (2017) 2306–2314.
[59] B. Zhao, K. Sun, F. Xue, J. Ouyang, Org. Electron. 13 (2012) 2516–2524.
[60] G.P. Dunn, L.J. Old, R.D. Schreiber, Annu. Rev. Immunol. 22 (2004) 329–360.
[61] H. Lee, H. Mok, S. Lee, et al., J. Control. Release 119 (2007) 245–252.
[62] Y. Cai, Q. Tang, X. Wu, et al., ACS Appl. Mater. Interfaces 8 (2016) 10737–10742.
[63] Y. Cai, Q. Tang, X. Wu, et al., ChemistrySelect 1 (2016) 3071–3074.
[64] P. Liang, J. Shao, Q. Tang, et al., RSC Adv. 7 (2017) 37369–37373.
[65] H. Shi, W. Sun, C. Liu, et al., J. Mater. Chem. B 4 (2016) 113–120.
[66] G. Liu, J. Zou, Q. Tang, et al., ACS Appl. Mater. Interfaces 9 (2017) 40077–40086.

[67] Y. Cai, P. Liang, Q. Tang, et al., ACS Appl. Mater. Interfaces 9 (2017) 30398–30405.
[68] Y. Liu, Z. Qu, H. Cao, et al., ACS Nano 11 (2017) 12446–12452.
[69] S. Huang, S. Liu, K. Wang, et al., Nanoscale 7 (2015) 889–895.
[70] J. Shao, Z. Guan, Y. Yan, et al., J. Org. Chem. 76 (2011) 780–790.
[71] H. Zhou, Y.L. Xiao, X.C. Hong, Chin. Chem. Lett. 29 (2018) 1425–1428.
[72] X. Luo, J. Li, J. Zhao, et al., Chin. Chem. Lett. 30 (2019) 839–846.
[73] Y. Cai, P. Liang, Q. Tang, et al., ACS Nano 11 (2017) 1054–1063.
[74] Y. Cai, P. Liang, W. Si, et al., Org. Chem. Front. 5 (2018) 98–105.
[75] P. Liang, Y. Wang, P. Wang, et al., Nanoscale 9 (2017) 18890–18896.
[76] H. Shi, W. Sun, Q. Wang, et al., ChemPlusChem 81 (2016) 515–520.
[77] R. Wang, H. Chen, W. Yan, et al., Eur. J. Med. Chem. 190 (2020) 112109.
[78] E. Hillard, A. Vessieres, L. Thouin, et al., Angew. Chem. Int. Ed. 45 (2005) 285–290.
[79] P. Liang, Q. Tang, Y. Cai, et al., Chem. Sci. 8 (2017) 7457–7463.
[80] J. Yang, Y. Cai, Y.X. Zhou, et al., Dyes Pigm. 147 (2017) 270–282.
[81] S. Zong, X. Wang, W. Lin, et al., Bioconjugate Chem. 29 (2018) 2619–2627.
[82] X. Huang, R. Gu, J. Li, et al., Sci. China Chem. 63 (2019) 55–64.
[83] F. Wu, L. Chen, L. Yue, et al., ACS Appl. Mater. Interfaces 11 (2019) 21408–21416.
[84] J. Zou, Z. Yin, P. Wang, et al., Chem. Sci. 9 (2018) 2188–2194.
[85] X. Yang, N.N. Shi, L. Bai, et al., Dyes Pigm. 157 (2018) 396–404.
[86] Q. Wang, B. Xia, J.Z. Xu, et al., Mater. Chem. Front. 3 (2019) 650–655.
[87] K.E. Washington, J. Du, R.N. Kularatne, et al., Synth. Met. 256 (2019) 116123.
[88] Q. Wang, Y.N. Dai, J.Z. Xu, et al., Adv. Funct. Mater. 29 (2019) 1901480.
[89] C. Wu, X. Huang, Y. Tang, et al., Chem. Commun. 55 (2019) 790–793.
[90] M. Grzybowski, V. Hugues, M. Blanchard-Desce, D.T. Gryko, Chemistry 20 (2014) 12493–12501.
[91] J. Zou, L. Xue, N. Yang, et al., Mater. Chem. Front. 3 (2019) 2143–2150.
[92] P. Liang, X. Huang, Y. Wang, et al., ACS Nano 12 (2018) 11446–11457.
[93] Y. Wang, X. Huang, Y. Tang, et al., Chem. Sci. 9 (2018) 8103–8109.
[94] H. He, X. Zheng, S. Liu, et al., Nanoscale 10 (2018) 10991–10998.
[95] V. Nguyen, Y. Yan, J. Zhao, J. Yoon, Acc. Chem. Res. 54 (2021) 207–220.
[96] Y. Xu, C. Li, R. Xu, et al., Chem. Sci. 11 (2020) 8157–8166.
[97] Z. Wang, Q. Peng, X. Huang, et al., Dyes Pigm. 185 (2021) 108877.
[98] L. Xue, Q. Shen, T. Zhang, et al., Mater. Chem. Front. 5 (2021) 6061–6070.
[99] N. Shi, Y. Shi, J. Shao, et al., Dyes Pigm. 160 (2019) 683–691.
[100] J. Shao, J. Chang, C. Chi, Chem. Asian. J. 9 (2014) 253–260.
[101] M. Weng, X. Yang, Y. Ni, et al., Sens. Actuators B 283 (2019) 769–775.
[102] S. Huang, C.J. Yang, J. Huang, et al., Dyes Pigm. 154 (2018) 269–274.
[103] Q. Zhu, M. Saeed, R. Song, et al., Chin. Chem. Lett. 31 (2020) 1051–1059.
[104] W. Yu, M. Shevtsov, X. Chen, H. Gao, Chin. Chem. Lett. 31 (2020) 1366–1374.
[105] Z. Shi, Q. Li, L. Mei, Chin. Chem. Lett. 31 (2020) 1345–1356.
[106] X. Ma, S. Bai, X. Zhang, et al., Biomacromolecules 20 (2019) 2637–2648.
[107] S. Bai, X. Ma, X. Shi, et al., ACS Appl. Mater. Interfaces 11 (2019) 36130–36140.
[108] D. Chen, X. Qu, J. Shao, et al., J. Mater. Chem. B 8 (2020) 2990–3004.
[109] Z. Li, C. Di, S. Li, et al., Acc. Chem. Res. 52 (2019) 2703–2712.
[110] Y. Wu, M. Yuan, J. Song, et al., ACS Nano 13 (2019) 8505–8511.
[111] J. Zhang, M. Zheng, F. Zhang, et al., Chem. Mater. 28 (2016) 8825–8833.
[112] L. Shen, T. Zhou, Y. Fan, et al., Chin. Chem. Lett. 31 (2020) 1709–1716.